



Characteristics of liquids lugs in gas-liquid Taylor flow in microchannels

Petr Zaloha, Jiri Kristal, Vladimir Jiricny, Norbert Völkel, Catherine Xuereb,
Joelle Aubin

► To cite this version:

Petr Zaloha, Jiri Kristal, Vladimir Jiricny, Norbert Völkel, Catherine Xuereb, et al.. Characteristics of liquids lugs in gas-liquid Taylor flow in microchannels. *Chemical Engineering Science*, 2012, vol. 68, pp. 640-649. 10.1016/j.ces.2011.10.036 . hal-00878423

HAL Id: hal-00878423

<https://hal.science/hal-00878423>

Submitted on 30 Oct 2013

HAL is a multi-disciplinary open access archive for the deposit and dissemination of scientific research documents, whether they are published or not. The documents may come from teaching and research institutions in France or abroad, or from public or private research centers.

L'archive ouverte pluridisciplinaire **HAL**, est destinée au dépôt et à la diffusion de documents scientifiques de niveau recherche, publiés ou non, émanant des établissements d'enseignement et de recherche français ou étrangers, des laboratoires publics ou privés.



Open Archive TOULOUSE Archive Ouverte (OATAO)

OATAO is an open access repository that collects the work of Toulouse researchers and makes it freely available over the web where possible.

This is an author-deposited version published in : <http://oatao.univ-toulouse.fr/>
Eprints ID : 10010

To link to this article : doi:10.1016/j.ces.2011.10.036
URL : <http://dx.doi.org/10.1016/j.ces.2011.10.036>

To cite this version : Zaloha, Petr and Kristal, Jiri and Jiricny, Vladimir and Völkel, Norbert and Xuereb, Catherine and Aubin, Joelle
Characteristics of liquids lugs in gas–liquid Taylor flow in microchannels. (2012) Chemical Engineering Science, vol. 68 (n° 1). pp. 640-649. ISSN 0009-2509

Any correspondance concerning this service should be sent to the repository administrator: staff-oatao@listes-diff.inp-toulouse.fr

Characteristics of liquid slugs in gas–liquid Taylor flow in microchannels

Petr Zaloha ^a, Jiri Kristal ^a, Vladimir Jiricny ^a, Norbert Völkel ^{b,c}, Catherine Xuereb ^{b,c}, Joelle Aubin ^{b,c,*}

^a Institute of Chemical Process Fundamentals of the ASCR, v.v.i., Rozvojova 135, CZ-165 02 Prague 6, Czech Republic

^b Université de Toulouse, INPT, UPS, Laboratoire de Génie Chimique, 4 Allée Emile Monso, BP-84234, 31030 Toulouse, France

^c CNRS, Laboratoire de Génie Chimique, 31030 Toulouse, France

ABSTRACT

The hydrodynamics of liquid slugs in gas–liquid Taylor flow in straight and meandering microchannels have been studied using micro Particle Image Velocimetry. The results confirm a recirculation motion in the liquid slug, which is symmetrical about the center line of the channel for the straight geometry and more complex and three-dimensional in the meandering channel. An attempt has also been made to quantify and characterize this recirculation motion in these short liquid slugs ($L_s/w < 1.5$) by evaluating the recirculation rate, velocity and time. The recirculation velocity was found to increase linearly with the two-phase superficial velocity U_{TP} . The product of the liquid slug residence time and the recirculation rate is independent of U_{TP} under the studied flow conditions. These results suggest that the amount of heat or mass transferred between a given liquid slug and its surroundings is independent of the total flow rate and determined principally by the characteristics of the liquid slug.

Keywords:
Hydrodynamics
Mixing
Multiphase flow
Microreactor
Gas–liquid
Micro-PIV

1. Introduction

Over the last decade, micro-reaction technology has become of much interest to both academics and the process industries for the intensification of chemical processes. Due to the extremely high surface to volume ratio and the small characteristic dimension of these devices, heat and mass transfer are remarkably intensified and the temperature within can be tightly controlled. These features of microreactors are particularly interesting for fast and highly exothermic gas–liquid reactions – amongst other applications – allowing an increase in the selectivity of the reaction whilst working in safe operating conditions. Several research studies have demonstrated that gas–liquid microreactors have unique advantages for various and some typically dangerous gas–liquid reaction systems, such as gas absorption (TeGrotenhuis et al., 2000; Yue et al., 2007), the direct synthesis of hydrogen peroxide (Inoue et al., 2007), direct fluorination (Jahnisch et al., 2000; Chambers et al., 2001; de Mas et al., 2003), three-phase hydrogenation reactions (Losey et al., 2001; Yeong et al., 2003; Kobayashi et al., 2004; Abdallah et al., 2004, 2006) and photochemical gas–liquid reactions (Ehrich et al., 2002).

A review of the current literature reveals that a number of different microreactors exist for implementing gas–liquid

reactions and their potential for highly exothermic and difficult chemistry has been well demonstrated (see Hessel et al., 2005). Many of the reported studies on gas–liquid flows in microreactors have concentrated on the evaluation of reaction performance, highlighting the advantages of micro-reaction technology for such applications, whereas less attention has been paid to the fundamental transport phenomena occurring and their interplay with chemical kinetics. Despite the successful demonstrations presented in the literature, controlling the flow regime and the characteristic size of the gas–liquid dispersion remains a difficult task. These parameters depend not only on the physical properties of the fluids (e.g. viscosity, density, interfacial tension) but also on the operating conditions, the geometry of the microreactor and the properties of the construction material (e.g. wettability, roughness). Although a range of advanced experimental techniques and computational approaches exist for evaluating mixing and flow in microreactors (Fletcher et al., 2009; Aubin et al., 2010), there is still a lack of detailed engineering principles for the design and operation of gas–liquid devices.

Up until now, much research on gas–liquid flow in microchannels has been dedicated to the study of flow patterns and the construction of flow pattern maps based on superficial gas and liquid velocities in circular, rectangular and triangular cross-section (e.g. Triplett et al., 1999; Chung and Kawaji, 2004; Serizawa et al., 2002; Cubaud and Ho, 2004; Kawahara et al., 2002; Waelchli and von Rohr, 2006; Yue et al., 2007, 2008). Depending on the operating conditions, the fluid properties and the microreactor geometry, different gas–liquid flow regimes can

* Corresponding author at: Université de Toulouse, INPT, UPS, Laboratoire de Génie Chimique, 4 Allée Emile Monso, BP-84234, 31030 Toulouse, France.

E-mail address: joelle.aubincano@ensiacet.fr (J. Aubin).

be obtained, including bubbly flow, slug or Taylor flow, slug-annular flow, annular flow and churn flow. Amongst these, slug or Taylor flow occupies the largest region on the flow regime map and appears at low to average gas and liquid flow rates. The gas-liquid Taylor dispersion in microchannels is extremely regular and is characterized by bubbles separated by slugs of liquid. The bubbles occupy almost the entire channel cross-section and are separated from the channel wall by a thin liquid film. Taylor flow is considered as a promising flow regime for gas-liquid chemical reaction in microreactors for two reasons: it is generated over a large range of gas and liquid flow rates, making the process operating conditions very flexible; and the physical flow pattern provides high interfacial area and velocity fields that are extremely interesting for process intensification.

Several studies in the literature have focused specifically on the hydrodynamics of gas-liquid Taylor flow in microchannels. Some of these deal with the effects of different process parameters (e.g. gas-liquid flow rates, fluid properties, microchannel geometry) on bubble formation and length using high speed visualization techniques (Garstecki et al., 2006; van Steijn et al., 2007; Yue et al., 2008; Yun et al., 2010, Leclerc et al., 2010, Abadie et al., 2011). Other studies have focused on attaining detailed information on hydrodynamics of the gas-liquid dispersion. These studies have employed micro Particle Image Velocimetry (micro-PIV) (Waelchli and von Rohr, 2006; Fries et al., 2008; Günther et al., 2004) and computational fluid dynamics (Fukagata et al., 2007; Fries and von Rohr, 2009) to investigate the flow patterns predominantly within the liquid slug. Globally, these studies confirm the existence of the recirculation motion in the liquid slug, which can be symmetrical or asymmetrical around the center line of the microchannel depending on the operating conditions and the topological geometry of the channel. Günther et al. (2004) showed that the recirculation motion within the liquid slug in a straight channel is in general symmetrical about the channel axis, which is consistent with Taylor's, 1961 prediction for liquid circulation in segmented flows in macroscopic systems. However, close scrutiny of the flow fields indicates some slightly non-symmetrical motion and the authors have attributed this to minor surface roughness effects, which become important at small scales, and the compressibility of the gas-phase. In the case of gas-liquid flow in meandering microchannels, the same authors found that the recirculation motion is asymmetrical and the two-dimensional streamlines are shown to be open loops, suggesting a three-dimensional flow. The authors also showed that the recirculating movement improved the mixing performance in the liquid slug in both the straight and meandering geometries compared with single phase liquid mixing in a channel. Furthermore, as the asymmetry of the flow increased, the channel length required for mixing decreased. More recently, Fries et al. (2008) and Fries and von Rohr (2009) have shown that the asymmetry of the recirculation loops in liquid slugs in meandering channels depends on the channel dimensions, the radius of curvature, the turning angle, as well as the superficial velocities of the gas and liquid. In their first paper, they characterized the strength of the recirculation motion with vorticity and swirling strength calculated from the micro-PIV data. The results show that the strength of the recirculating motion can be enhanced by decreasing the radius of

curvature of the channel bend. On the other hand, an increase in superficial velocity – either by increasing the flow rate or by decreasing the channel diameter – leads to an increase in the size of high vorticity zones without increasing the magnitude of vorticity. Further micro-PIV experiments and 2-dimensional CFD simulations have shown how the recirculation velocity field changes as a function of superficial velocity and the radius of curvature (Fries and von Rohr, 2009). The microchannel bend induces an asymmetrical flow pattern such that in some cases the recirculation loops are positioned diagonally in the liquid slug and in other cases, the outer recirculation loop splits into two or even disappears. These results all give qualitative insight into how liquid mixing is improved in gas-liquid segmented flows. von Rohr's group has also used micro-PIV to investigate the effects of the physical properties of the fluids on the recirculation of the liquid phase in gas-liquid flows in a straight microchannel (Waelchli and von Rohr, 2006). Their results suggest that the recirculation motion within the liquid phase is affected more so by the interfacial forces than the liquid viscosity. In fact, the interfacial tension between the gas and liquid phases determines in part the shape of the leading and trailing edges of the bubbles, which in turn affects the liquid recirculation flow pattern. In a recent study, Fouilland et al. (2010) have used high speed micro-PIV to obtain liquid velocity profiles in the liquid film and/or the liquid slug in Taylor, as well as slug-annular and annular flows in microchannels. In Taylor flow, they found that the highest velocities measured in the liquid film when a bubble is passing are at least 20 times less than those at the same location when a liquid slug is passing. This suggests that the liquid slug acts like a piston and significantly accelerates the liquid film that was surrounding the bubble. Once the slug has passed, the velocity of the liquid film drops back to its initial value.

The objective of this study is to better understand and characterize the recirculation motion in the liquid slug of gas-liquid Taylor flow in a straight microchannel section and different shaped bends of a meandering microchannel via micro-PIV measurements. The study also aims at developing a methodology for analyzing the recirculation motion in the liquid slug and determining characteristic values such as the recirculation flow rate, velocity and time, which are necessary for better understanding of the transport processes in gas-liquid Taylor flow in microreactors and developing phenomenological models.

2. Experimental methods

2.1. Experimental set-up

Gas-liquid Taylor flow was generated in a rectangular cross-section microchannel. The gas and liquid phases are contacted using a side-entering T-junction geometry and the main channel has a meandering form with right-angled or curved bends, as shown in Fig. 1. The width of the main channel, w , is 1000 μm , the width of the side entering the channel, w_{in} , for the gas phase is 525 μm and the channel depth, h , is 400 μm . The entire length of the main channel is approximately 0.3 m. The microchannels were etched through a silicon wafer plate using the Deep Reactive



Fig. 1. Schematic diagram of the T-junction microchannel (left) and the topology of the curved (center) and right-angled (right) meandering microchannels.

Table 1

Summary of operating conditions and corresponding dimensionless numbers.

U_L (m/s)	U_G (m/s)	U_{TP} (m/s)	U_G/U_L	$\beta = U_G/U_{TP}$	Re_{TP}	$Ca_{TP} (\times 10^{-3})$
0.010	0.010	0.021	1.00	0.50	8	1.1
0.010	0.021	0.031	2.00	0.67	12	1.7
0.010	0.031	0.042	3.00	0.75	16	2.3
0.010	0.042	0.052	4.00	0.80	20	2.8
0.021	0.021	0.042	1.00	0.50	16	2.3
0.021	0.031	0.052	1.50	0.60	20	2.8
0.021	0.042	0.063	2.00	0.67	24	3.4
0.031	0.031	0.063	1.00	0.50	24	3.4
0.031	0.042	0.073	1.33	0.57	28	3.9
0.042	0.042	0.083	1.00	0.50	32	4.5

Ion Etching technique and sandwiched between two Pyrex glass wafers using anodic bonding.

The liquid was fed to the main microchannel using a Harvard apparatus PHD 2000 syringe pump and the gas flow rate was controlled by a HoribaStec SEC-7320 mass flow controller. Ethanol and air at ambient temperature and pressure were used as the liquid and gas phases, respectively. Table 1 summarizes the operating conditions employed. The superficial velocities for both phases varied between 0.010 m/s and 0.042 m/s (i.e. 0.25 ml/min and 1.00 ml/min) such that the effect of different superficial velocity ratios and two phase velocity could be studied. These operating conditions correspond to liquid Reynolds numbers (based on the total superficial velocity) ranging from 8 to 32 and Capillary numbers ($Ca_{TP} = \mu_L U_{TP} / \sigma_L$) of the order of 10^{-3} . The liquid slug length varied between 0.85 and 1.45 mm and its dependency on the flow rate ratio is shown in Fig. 10.

2.2. Visualization and micro-PIV experiments

The bubble and liquid slug lengths as well as the bubble velocities were measured using high-speed camera visualization. A Photron FASTCAM 1.1 CMOS camera was used to image the bubbles at a frame rate of 1000 fps. A Matlab program was then used to determine the bubble velocity from consecutive image pairs. For every gas–liquid flow rate combination, the average bubble and slug lengths and bubble velocities were determined from a total of 1500 images.

The absolute liquid flow velocity fields in a two-dimensional plane perpendicular to the channel cross-section between two Taylor bubbles were obtained by micro-PIV. Measurements were made for several flow rate combinations in the straight section of the microchannel and for one pair of gas and liquid flow rates in the bend of the microchannel. The micro-PIV system employed consisted of a CCD camera (LaVision Imager Intense, 12-bit double exposure, 10 Hz, 1376×1040 pixels²), an inverted microscope (Axiovert 200M, Zeiss) and a double-pulsed Nd:YAG laser with a wavelength of 532 nm. The camera and the laser pulses were synchronized using a Programmable Timing Unit. The liquid was seeded with monodisperse rhodamine-doped polymer particles with a diameter of 2.81 μm (MicroParticles GmbH). A 5 \times objective mounted on the microscope enabled the visualization of the seeding particles in a field of view of approximately 2×2 mm with an out-of-plane resolution of about 250 μm . For the velocity measurements, the focal plane of the microscope with the 5 \times objective was positioned at mid-channel height. For every combination of gas and liquid flow rates, 650 image pairs were recorded.

The absolute velocity fields were calculated using the DaVis 7 software (LaVision). Ensemble averaged velocity fields in the liquid slug for fixed bubble positions were calculated using the sum of correlation algorithm. Using this algorithm, the absolute velocity field was calculated by applying a cross-correlation between image frames in a multipass mode, that is using iterative calculations with

decreasing window size from 64×64 pixels² (2 passes) to 32×32 pixels² (1 pass), both window sizes having 50% overlap. The relative velocity fields were determined by subtracting the bubble velocity from the absolute liquid velocity field.

2.3. Calculation of recirculation flow characteristics

The velocity fields obtained by micro-PIV were further analyzed to extract quantitative information on the recirculation flow in the liquid slug between two bubbles. In particular, approximate values of the rate of flow recirculation, the recirculation velocity and the recirculation time were determined. This information is useful for the evaluation of transport processes such mixing, and mass and heat transfer. In order to obtain this quantitative characteristic information on the recirculation flow in the liquid slug, a simplified methodology for the analysis of the two-dimensional velocity data has been developed and is described below. Under the adopted simplifying assumptions, this approach provides approximate values of the recirculation characteristics, as well as insight on the evolution of these values with operating conditions that can be used for engineering design purposes.

Using the two-dimensional relative liquid velocity field measured between two bubbles, the velocity profile along a line that passes through the center of the recirculation loop is extracted and plotted against the dimensionless channel width, as shown in Fig. 2(a). A symmetrical velocity profile is calculated as the mean of the left and right halves of the experimental velocity profile and is then

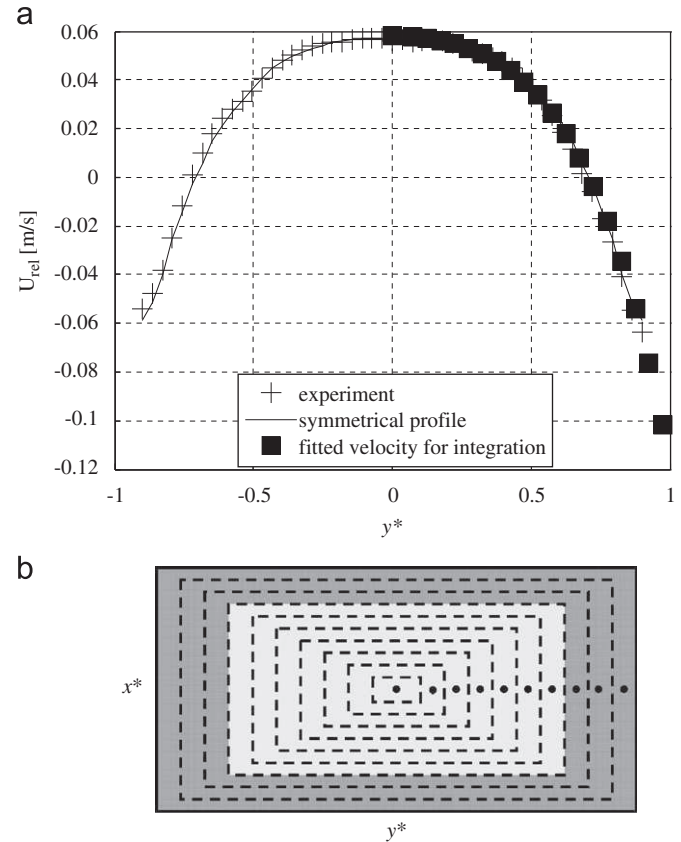


Fig. 2. (a) Extraction of a relative velocity profile (from the micro-PIV velocity field) midway between two bubbles and an example of this velocity profile compared with the symmetrical mean profile and fitted data ($U_G=0.042$ m/s, $U_L=0.042$ m/s). (b) Discretization of the microchannel cross-section into rectangular rings with equal aspect ratio. The light gray shaded area corresponds to flow rate Q_1 and the dark gray shaded area corresponds to Q_2 , which is flowing in the opposite direction to the main flow.

fitted with a polynomial. The rate of flow recirculation is calculated by carrying out a surface integration of the velocity profile across the microchannel cross-section, similarly to what is done in conventional stirred tanks to calculate circulation induced by the mechanical impeller (Jaworski et al., 1996). To do this, the microchannel cross-section is discretized into a number of rectangular rings with equal aspect ratios as shown in Fig. 2(b). This is a simplified representation of the iso-velocity contours of laminar flow in a rectangular duct and reasonable approach for the scope of this study. Using the symmetrical velocity profile, a velocity is assigned to each one of the rectangular rings. In this approach, it is assumed that the velocity is same at every point in a single rectangular ring. It is true that in the case of long liquid slugs ($L_s/w \gg 1$), the core of the slug is assumed to have a parabolic flow profile and the theoretical velocity profile for laminar flow in rectangular ducts can be used to obtain a more accurate estimation of the quantitative recirculation characteristics. However, for liquid slugs that are approximately equal to or shorter than the characteristic dimension of the channel, there is significant interaction between the leading and trailing menisci of the liquid slug and the velocity field within the slug is modified, especially at finite values of the Reynolds number (Fujioka and Groberg, 2004). In such cases, the flow cannot be approximated by the usual parabolic profile and experimental or numerical data are needed to evaluate the characteristic values of the recirculation flow.

As depicted in Fig. 2, the surface integration of the relative velocity profile generates two flow rates: a positive flow rate in central core of the microchannel, Q_1 , that is in the direction of the main flow and a negative flow rate, Q_2 , that corresponds to the recirculating liquid close to the microchannel walls. The recirculation flow rate, Q_{rc} , is then defined as

$$Q_{rc} = Q_1 \quad (1)$$

Q_2 is equal to Q_1 if there is no liquid film and the entire volume of the liquid slug recirculates. In the case of a relatively thick liquid film, Q_2 will be greater than Q_1 . This is evidence of bypass flow in the liquid film that does not participate in the recirculation flow within the liquid slug and therefore reduces the effective recirculation volume. The average recirculation velocity is defined as

$$U_{rc} = \frac{Q_{rc}}{A_{Q_1}}, \quad (2)$$

where A_{Q_1} is the cross-sectional area occupied by flow rate Q_1 . The characteristic recirculation time is the time required for an element of liquid to complete one revolution in the recirculating liquid slug and is calculated as

$$t_{rc} = \frac{V_{rc}}{Q_{rc}} \quad (3)$$

When the liquid film is very thin or nonexistent, $Q_2 \approx Q_1$ and the recirculating volume V_{rc} occupies the entire cross-section of the microchannel. In this case, V_{rc} can be roughly approximated as the volume of liquid between two bubble caps. If $Q_2 > Q_1$ due to a non-negligible liquid film and the presence of bypass flow, the recirculation volume occupies only part of the microchannel cross-section. Q_2 can then be divided into two parts, $Q_{2,s}$ and $Q_{2,f}$, which contribute to the recirculation in the slug and the flow in the film, respectively. When $Q_2 > Q_1$, the recirculating volume V_{rc} is defined as the sum of the volumes occupied by flow rates Q_1 and $Q_{2,s}$.

3. Results and discussion

3.1. Velocity fields in the liquid slug

Fig. 3(a) shows the normalized liquid velocity (U_{abs}/U_{TP}) profiles across the microchannel, midway between two bubbles.

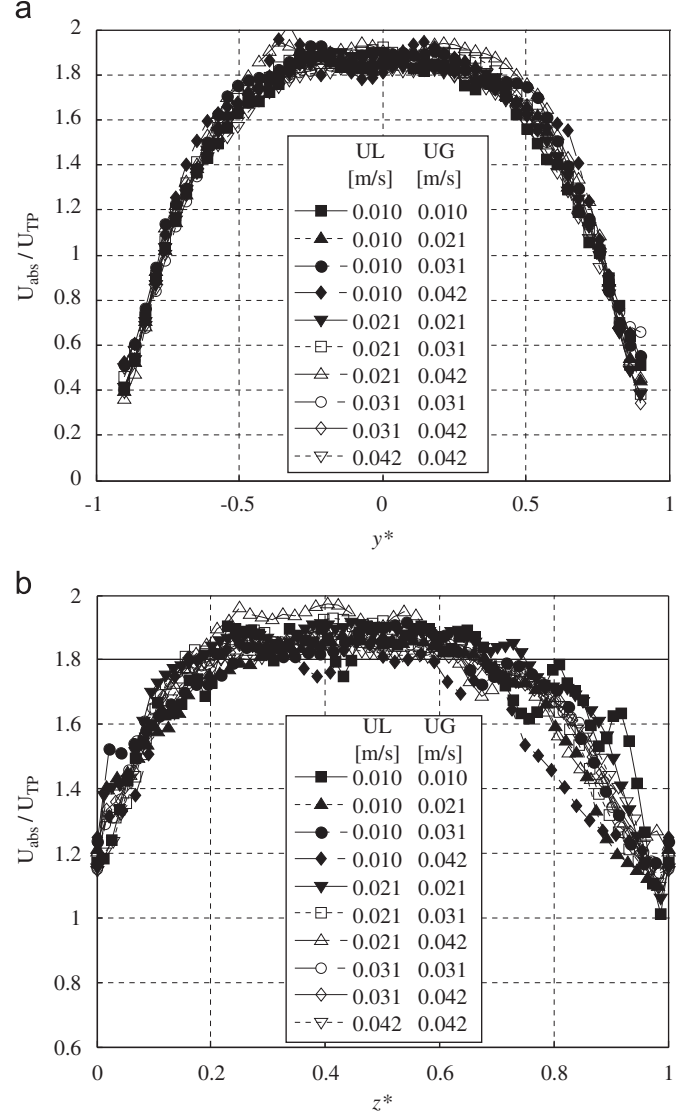


Fig. 3. (a) Normalized velocity profiles across the microchannel in the middle of the liquid slug for the different operating conditions. (b) Normalized liquid profiles along the center of the liquid slug for different operating conditions.

The velocity profiles are very consistent for all operating conditions used and are also symmetrical about the channel center line. Fig. 3(b) shows the normalized liquid velocity profiles along the center of the liquid slug for the various operating conditions. The flow direction is from left to right, thus $z^*=0$ corresponds to the axial-position in line with the bubble nose (rear end of the liquid slug) and $z^*=1$ corresponds to the axial-position in line with the rear end of the bubble (liquid slug nose). These normalized velocity profiles collapse very well from $z^*=0$ to $z^*=0.6$ for all operating conditions, however some deviations are observed in the leading third of the liquid slug ($z^*=0.6$ to $z^*=1$). In a general manner, the center line velocity of the liquid slug is approximately equal to U_{TP} at the rear of the bubble, increases to about $2U_{TP}$ along the bulk of the slug and then decreases to about $1.2U_{TP}$, which is very close to U_b , just in front of the following bubble nose.

Fig. 4(a) shows an example of the liquid velocity field between two Taylor bubbles in a straight section of the microchannel for equal gas and liquid superficial velocities of 0.042 m/s in the frame of reference relative to the bubble. The velocity fields obtained with other operating conditions are qualitatively similar, with variations in flow intensity and slug length. In a general

manner, the flow within the liquid slug is characterized by a central core of fluid moving in the direction of the main gas–liquid flow and zero velocity at the front and rear end of the

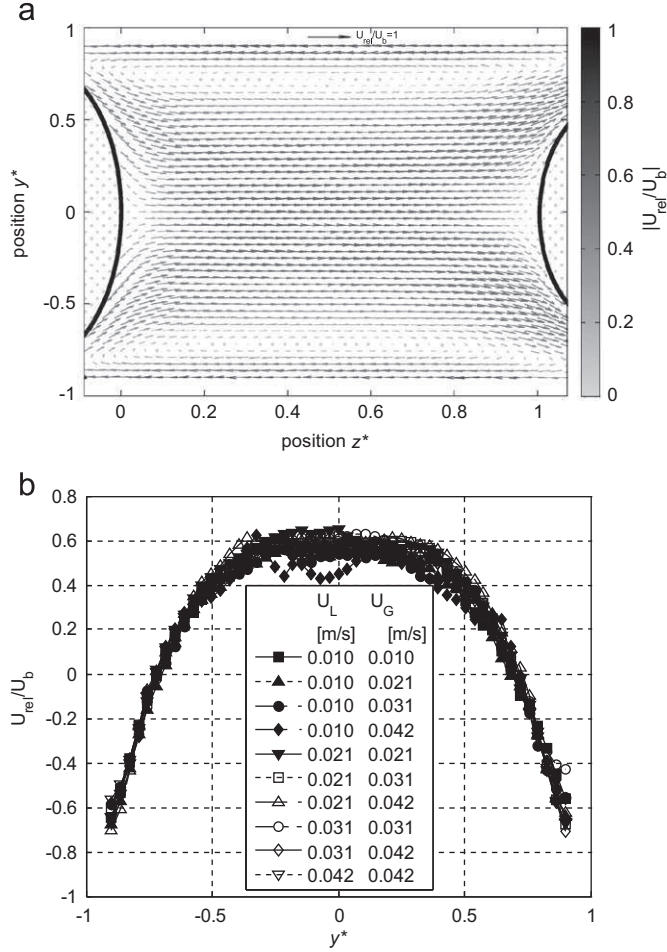


Fig. 4. (a) Relative velocity field in the liquid slug between two Taylor bubbles for superficial velocities $U_G=0.042$ m/s and $U_L=0.042$ m/s (flow is from left to right); (b) Dimensionless relative velocity profiles across the channel midway between two bubbles for different flow rate conditions.

bubbles, which causes a reverse flow close to the microchannel walls. In a two-dimensional representation, as is the case of the vector plot shown in Fig. 4(a), this recirculation flow behavior is characterized by two recirculation loops. In 3-dimensions, however, the recirculation motion is expected to take a torus-like shape, which is distorted somewhat according to the cross-sectional shape of the microchannel.

Fig. 4(b) shows the dimensionless relative velocity (U_{rel}/U_b) profiles across the channel, midway between two bubbles for different flow rate conditions. From these profiles it is possible to determine the radial position of the vortex center, i.e. the point at which flow reversal occurs. The center of the recirculation loops in the liquid slug is defined at point where the relative liquid velocity is zero and for the range of operating conditions studied here, it is found to be at approximately $y^*=0.72$. This value is in very good agreement with the theoretical value of 0.716 that is calculated using the laminar velocity profile in rectangular ducts given by Shah and London (1978).

An example of the relative velocity fields of the liquid slug moving through a curved bend in the microchannel are presented in Fig. 5. For this case, the direction of the gas–liquid flow is from the right to the left and the superficial velocities are $U_G=0.031$ m/s and $U_L=0.031$ m/s. The vector plots show that as the liquid slug goes through the bend, the recirculation patterns are modified compared with those generated in a straight section of microchannel. The flow pattern is asymmetrical with the recirculation loops positioned diagonally in the liquid slug; the circulation loop on the inner side of the bend has almost disappeared. These observations are in very good agreement with experimental and numerical work presented in the literature (Fries and von Rohr, 2009; Dogan et al., 2009), which has also shown the effectiveness of these complex flow patterns for mixing in the liquid slug. Although the Reynolds numbers in the present experiments are low, ranging from 8 to 32, the inertial effects on the flow are non-negligible in the bends of the meandering channels. Indeed, the generation of rotating flow features – known as Dean vortices – in channel and pipe bends are well known (Dean, 1927). Our previous work has shown that the geometry of these curved microchannels induces the formation of two Dean vortices in single phase flow in the range of Reynolds numbers studied here, thereby creating transverse and rotating flow normal to the main flow direction (Aubin et al., 2009). The recirculation flow within the liquid slug of the gas–liquid flow is

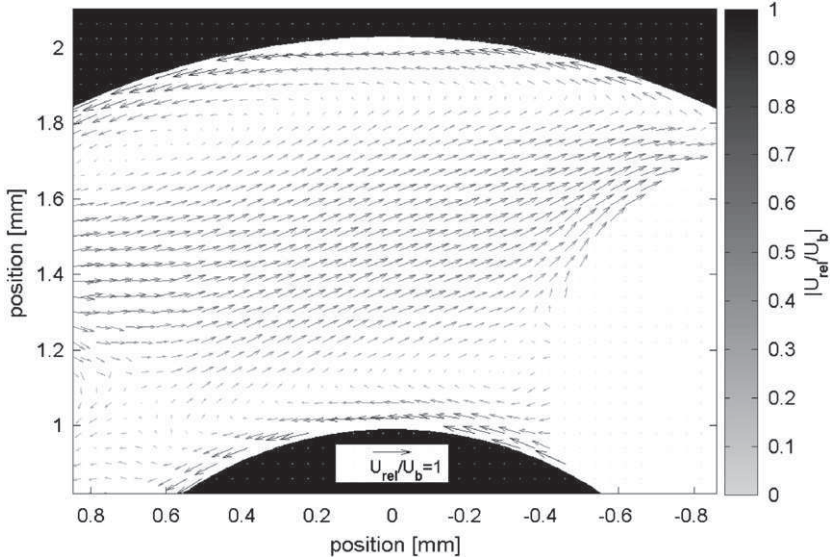


Fig. 5. Effect of the curved bend on the recirculation flow in the liquid slug between two Taylor bubbles for superficial velocities $U_G=0.031$ m/s and $U_L=0.031$ m/s. The flow direction is from the right to the left. Only every second vector is shown in the figures for clarity.

normal to the rotating flow of the Dean vortices. It is therefore not surprising that the combination both of these flow results in a complex three-dimensional flow, which is suggested by flow fields shown in Fig. 5.

The effect of a right angled bend of the microchannel on the recirculation flow in the liquid slug has been investigated by measuring the liquid velocity fields in the bend for 16 different bubble positions. The bubble positions are taken at different times, expressed as a dimensionless time, t^* , which is the time normalized by the bubble period. At $t^*=0$, the bubble is at the entry of the observed area. Fig. 6 shows the liquid velocity fields (relative to the bubble velocity) for 9 bubble positions taken at t^* intervals of approximately 0.1 and with superficial velocities $U_G=0.031 \text{ m/s}$ and $U_L=0.031 \text{ m/s}$. The direction of the gas-liquid flow is from top to right. When the bubble is just entering the microchannel bend, the recirculation flow in the liquid ahead of the bubble is somewhat similar to that observed in the straight channel section and characterized by two symmetrical circulation loops (Fig. 6(a)). The center of the recirculation loop, i.e. where the relative velocity is zero, does not follow the right-angled shape of the microchannel bend but a more rounded path, as if the microchannel bends were curved. In the lower corner of the channel bend, the absolute liquid velocities are close to zero and are therefore depicted as vectors with a normalized relative velocity, U_{rel}/U_b , of almost -1. As the bubble moves into and

through the bend, the bubble nose starts to push the liquid in an asymmetrical manner (Fig. 6(b)-(e)). In Fig. 6(e) and (f) it can be seen that even when the bubble body is in the bend, the bubble does not fill the channel and a significant proportion of bend is always filled with liquid. The vector plots qualitatively show that the liquid in the channel bend moves in the vicinity of the bubble but appears to be stagnant right in the corner. A quantitative analysis of this is given further on. As the bubble starts to move out of the bend, the relative liquid velocities increase in the reversely flowing liquid in the outer side of the bend and at the rear of the bubble (Fig. 6(f)-(h)). This is most likely due to a low pressure region created at the rear end of the bubble. As the bubble moves on, it can be seen that the recirculation flow immediately behind the bubble is more complex than that observed in the straight channel section, characterized by the formation of secondary recirculation loops close to the bubble tail (Fig. 6(h) and (i)). However, the principal recirculation pattern follows further upstream of the bubble. It is interesting to point out that this principal circulation pattern appears to be asymmetrical, with only one apparent loop close to the outer bend. The secondary loop close to the inner corner observed in Fig. 6(i) may in fact grow as the bubble moves down the channel to form a flow pattern that is symmetrical about the channel center line. These vector plots clearly show that the fluid flow in the microchannel bend is time dependent and highly 3-dimensional, which

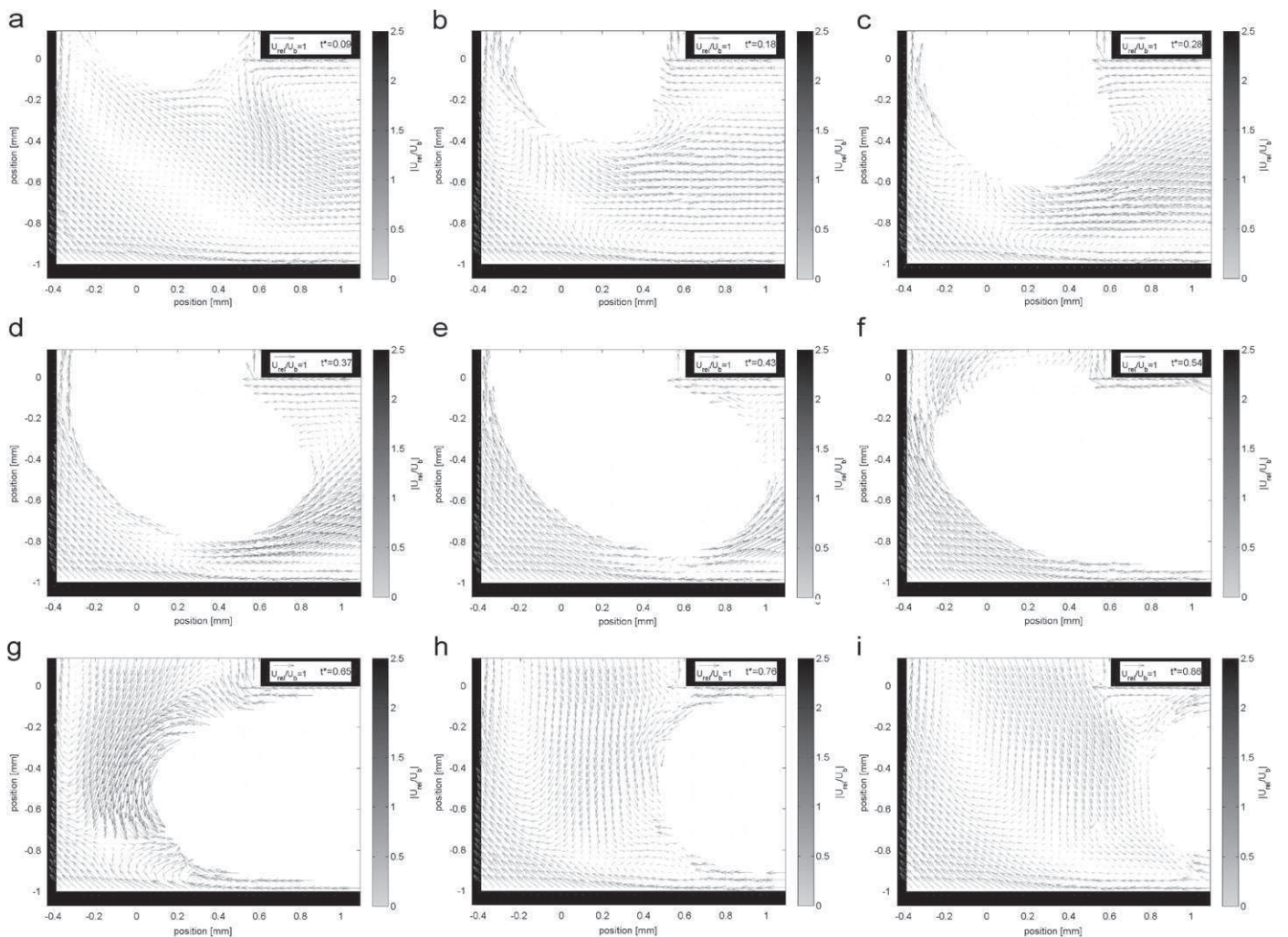


Fig. 6. Effect of a right angled bend on the recirculation flow in the liquid slug between two Taylor bubbles for superficial velocities $U_G=0.031 \text{ m/s}$ and $U_L=0.031 \text{ m/s}$. The flow direction is from the top to the right. Only every second vector is shown in the figures for clarity.

qualitatively explains the improved mixing observed in segmented flow in meandering channels (Günther et al., 2004).

The vector plots in Fig. 6 qualitatively show that there is a significant zone in the microchannel corner where gas is never present and that the circulation in this zone is limited, creating to some extent a dead zone where the transport phenomena may be hindered. Analysis of the liquid velocity vector plots in this zone for the 16 bubble positions (or t^* values) as shown in Fig. 7(a) that at the most, about a third of the diagonal distance across the microchannel corner (i.e. for $L_D < 0.31$) is not occupied by the gas phase when the bubble passes through the bend. In order to better quantitatively evaluate the extent of the dead zone in the microchannel bend, the normalized relative liquid velocity (U_{rel}/U_b) profiles have been plotted along a diagonal transect in the 'liquid only' zone for the 16 different bubble positions. The value of U_{rel}/U_b is -1 when the absolute liquid velocity is zero and is greater than zero where the liquid is moving faster than the bubble. Fig. 7(b) shows the velocity profiles along the transect for the 16 bubble positions (black lines) and the corresponding standard deviation of the velocity (dashed line). It can be seen that from the outer corner of the microchannel until approximately 10% of the diagonal distance ($L_D < 0.1$), the relative velocities are close to -1 for all bubble positions and that the standard deviation is close to zero. For $0.1 < L_D < 0.25$, however, there is significant variation in relative velocities depending on

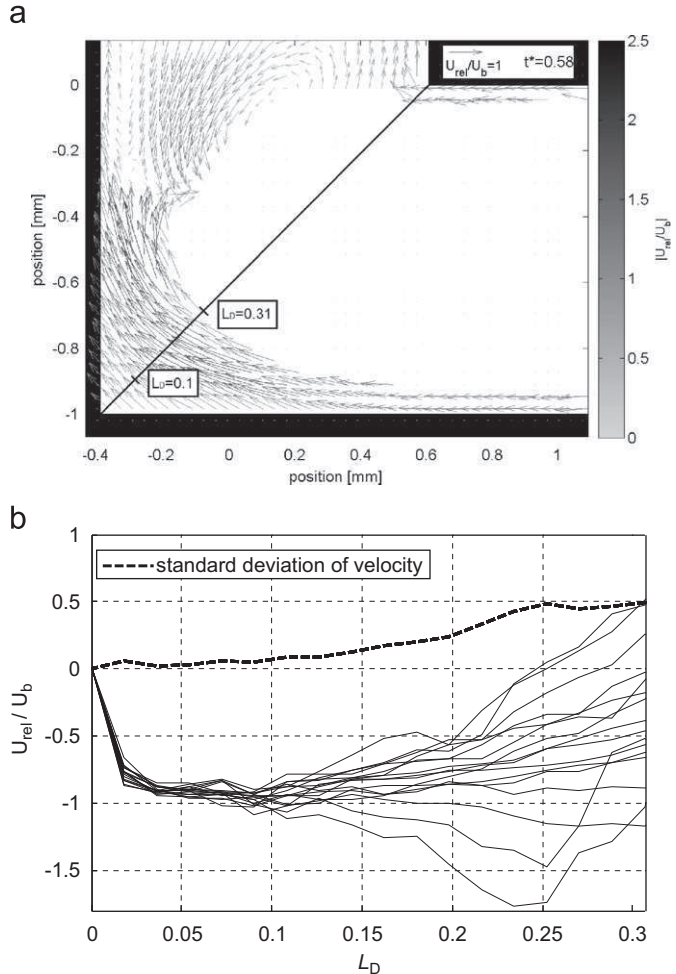


Fig. 7. Evaluation of the dead zone in the microchannel bend. (a) Diagonal transect across the microchannel bend along which velocity profiles are plotted. (b) Normalized relative velocity profiles (black lines) along the diagonal transect for 16 different bubble positions and corresponding standard deviation (dashed line).

the bubble position. This results in an increase of the standard deviation, which then reaches a plateau at a value of approximately 0.5 for $0.25 < L_D < 0.31$. From this analysis we consider the liquid in the microchannel corner to be stagnant when the standard deviation is less than 0.1. For the given geometry, this means that the dead zone extends to $L_D \sim 0.1$ and therefore only a very small zone of the corner can be considered truly stagnant. The remaining 'liquid only' zone ($0.1 < L_D < 0.31$) is not stagnant because the bubbles induce significant fluctuations in the liquid velocities and the flow direction, which are responsible for promoting mixing and mass transfer.

3.2. Recirculation characteristics of the liquid slug

Fig. 8(a) shows the recirculation velocity, U_{rc} , in the liquid slug as a function of the superficial velocity ratio, U_G/U_L . It is clear from this figure that the recirculation velocity does not correlate with the superficial velocity ratio. On the other hand, when the recirculation velocity is plotted as a function of the two-phase superficial velocity as shown in Fig. 8(b), all of the data collapse together. The recirculation velocity is linearly dependent on the total (gas and liquid) flow rate and thus on the two-phase superficial velocity U_{TP} . The ensemble of data show that U_{rc} is approximately $0.4U_{\text{TP}}$ for the conditions studied here.

The graph given in Fig. 8(b) can also be expressed in terms of characteristic times as presented in Fig. 9, which plots the recirculation time in the liquid slug as a function of the time required for a slug to move its own length, L_s/U_{TP} . It can be seen that the recirculation time is a linear function of L_s/U_{TP} and is therefore dependent on both the two phase flow rate and the gas-to-liquid flow rate ratio since the slug length is linearly dependent on $(U_G/U_L)^{-1}$ as shown in Fig. 10 following the Garstecki model for bubble lengths (Garstecki et al., 2006).

The data in Fig. 9 show that a fluid element completes one revolution in the liquid slug in the time required for the slug to travel five times its own length, i.e. $\sim 5L_s/U_{\text{TP}}$. Using a similar approach, Thulasidas et al. (1997) showed that for gas-liquid flow in capillary tubes at low Ca ($< 10^{-2}$), the time required for an element of fluid to move from one end of the liquid slug to the other end is constant and equal to $2.0L_s/U_{\text{TP}}$. Our result is in very good agreement with that of Thulasidas et al. (1997) since it is expected that the distance from one end of the slug to the other is slightly less than half the distance required to complete a full revolution of the liquid slug. It can also be said from Fig. 9 that for a constant total flow rate, the fluid in a shorter slug will undergo a larger number of revolutions compared with a longer slug. Furthermore, for a fixed slug length, the recirculation time becomes shorter as the total flow rate increases. This suggests that short slugs at high U_{TP} provide the most adequate recirculation conditions (high recirculation rates) for heat and mass transfer processes. However, once should keep in mind that although the fluid recirculation rate increases with increasing U_{TP} and constant slug length, the residence time in the microchannel decreases. This means that although shorter faster moving slugs will recirculate at a higher rate, the number of revolutions made in the slug over the length of the microreactor will not necessarily increase because of the shorter time spent in the microchannel.

Using the result of Fig. 9, it can be shown that the product of the recirculation rate and the residence time of a liquid slug in a fixed length of channel is dependent on the liquid slug length only. This is confirmed in Fig. 11, which shows that the total number of revolutions occurring in the slug along the entire microchannel is essentially constant (the slight scattering of data is attributed to the variations in slug length, $0.85 < L_s/w < 1.45$) regardless of the two-phase superficial velocity. This result

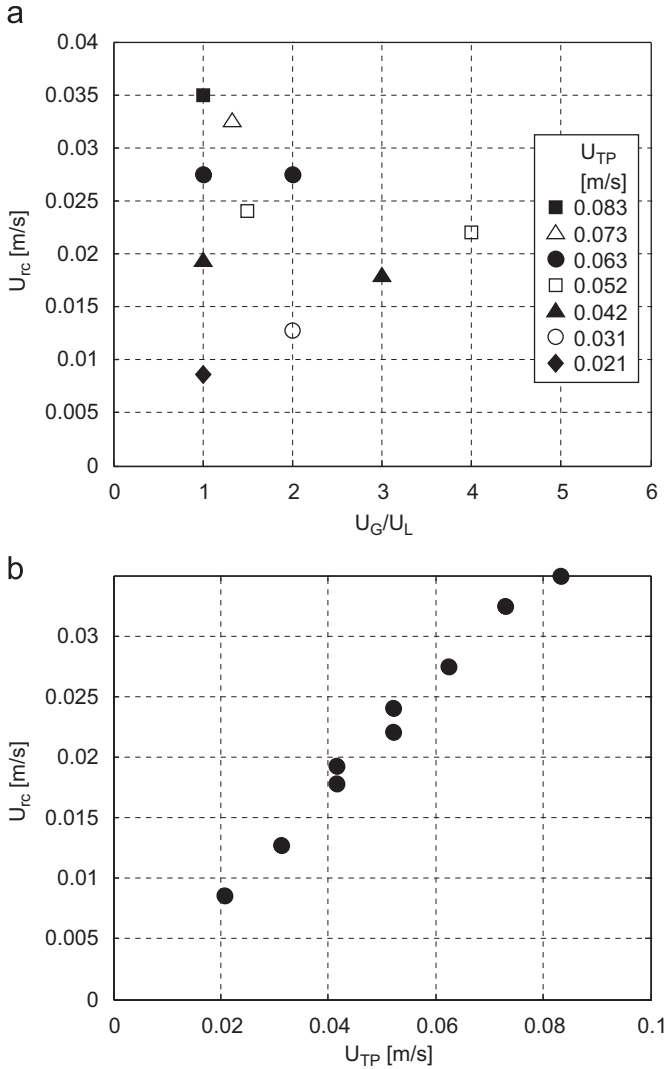


Fig. 8. (a) Recirculation velocity as a function of the superficial velocity ratio, U_G/U_L .
(b) Recirculation velocity as a function of the two-phase superficial velocity, U_{TP} .

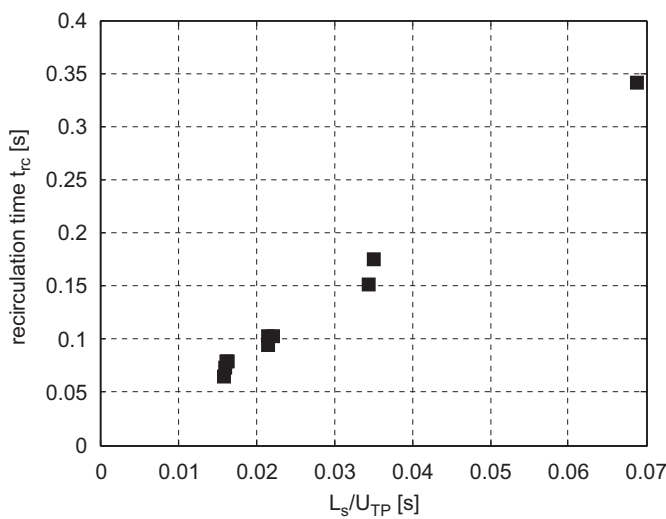


Fig. 9. Recirculation time as a function of the time needed for a liquid slug to move its length.

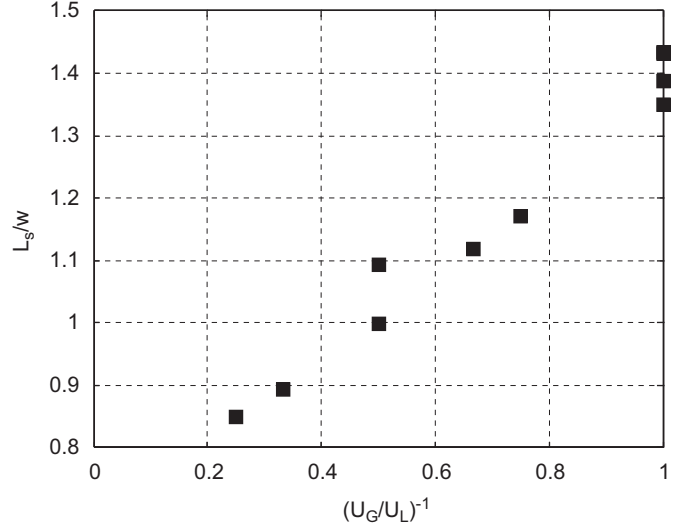


Fig. 10. Liquid slug length as a function of the superficial velocity ratio, $(U_G/U_L)^{-1}$.

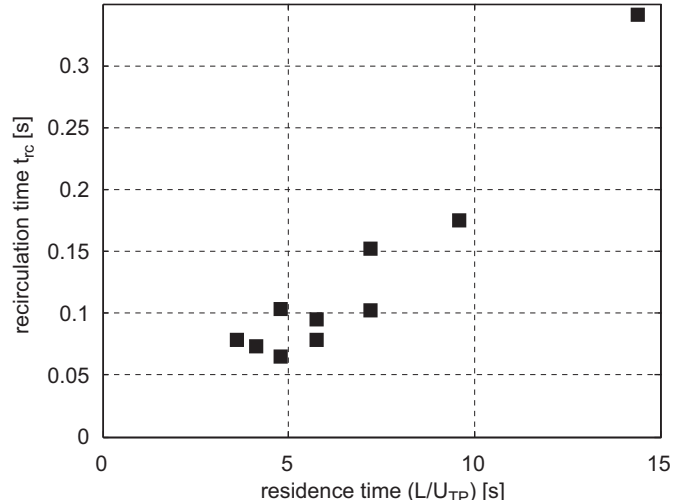


Fig. 11. Recirculation time as a function of the residence time of the liquid slug in the microchannel.

indicates that the amount of heat or mass transferred between a liquid slug (of fixed length) and its surroundings may therefore be constant and independent of total flow rate when the transport processes are controlled by the rate of recirculation. Indeed, Gupta et al. (2010) found that heat transfer was independent of U_{TP} for short slug lengths $L_s/d_H \sim 1$, which are similar to those in this study. However, the global transport process may not always be controlled by the rate of recirculation in the slug. Leung et al. (2010) found that heat transfer is also limited by the liquid phase hold-up. They showed that heat transfer in gas–liquid Taylor flow in microchannels is at its maximum for $0.1 < \beta < 0.3$ and the benefits of high recirculation rates in shorts slugs are outweighed when the amount of liquid available for heat transfer decreases below a certain limit. In a similar manner, it may be also expected that gas–liquid mass transfer be hindered if the liquid slugs are too short and therefore quickly saturated, decreasing thus the driving force for the transport process.

Although the results shown here demonstrate the independency of the recirculation rate on U_{TP} , this need not always be the case. The observations in this study were made for certain operating conditions, e.g. very short slug lengths ($L_s/w \sim 1$), low capillary numbers ($Ca \sim 10^{-3}$) and a straight microchannel section. However, as shown

in Figs. 5 and 6, the inertia in meandering geometries can have non-negligible effects on the flow in the liquid slug and it is expected that these flow characteristics are dependent on U_{TP} – like is the case for single phase flow – and may therefore lead to enhanced gas–liquid transport processes. Leung et al. (2010) have also shown that heat transfer can be significantly affected by U_{TP} in very long liquid slugs ($50 < L_s/d < 250$); this may be attributed to the very weak, almost nonexistent internal recirculation, the slugs that may be greatly enhanced by an increase in U_{TP} .

4. Conclusions

Micro-PIV measurements have been performed in gas–liquid Taylor flow in microchannels to determine the effects of flow rates and channel geometry on the liquid velocity fields. Using the flow data and a method adapted from traditional batch mixing analysis, the recirculation motion in the liquid slug has been quantified by evaluating the recirculation rate, velocity and time.

The measured velocity fields confirm the existence of circulation loops in the liquid slugs of gas–liquid Taylor flow in both straight and meandering microchannels. In the straight microchannel, the size of and the positions of the center of the recirculation loops are almost constant for the range of operating conditions investigated and they are symmetrical about the center line of the channel. In order to obtain recirculation patterns that demonstrate bypass flow with a reduced recirculation volume and vortex centers that are closer to the channel center line, the capillary number needs to be increased at least one or two orders of magnitude. This would typically require fluids with varying viscosity and/or surface tension to be used in the existing experimental setup. In meandering channels, the bends induce a highly three-dimensional flow that is non-symmetrical about the channel center line and dependent on the bubble position. A ‘liquid only’ zone (that is never occupied by bubbles) exists in the case of right-angled bend microchannels. This zone occupies about a third of the channel corner, however a quantitative analysis of the liquid in this area shows that the majority of the liquid in this area is in motion with fluctuating velocities. This enables us to conclude that the corner area in the microchannel is not entirely a dead zone and it is involved in heat and mass transport processes.

Quantification of the recirculating liquid slug shows that the recirculation velocity increases linearly with the two-phase superficial velocity U_{TP} and is independent of the superficial velocity ratio U_G/U_L for the studied conditions. On the other hand, the recirculation time is proportional to L_s/U_{TP} and proportional to the mean residence time of the liquid slug in the microchannel. These results show that short liquid slugs at high U_{TP} provide the highest recirculation rates but also that the number of fluid revolutions in the liquid slug of fixed length is independent of U_{TP} during the residence time in the microchannel. Within the range of conditions studied (i.e. short slug lengths, low capillary numbers, straight microchannel section), this suggests that efficiencies of heat and mass transfer processes between a single liquid slug and its surroundings in the microchannel may be determined principally by the characteristics of the liquid slug rather than U_{TP} . Indeed, to confirm the limits of this claim, further studies that explore the recirculation behavior at higher capillary numbers and the impact of the flow on the global heat and mass processes in the reactor will be required.

Nomenclature

A	cross-sectional area (m^2)
d_H	hydraulic diameter (m)

h	microchannel height (m)
L	microchannel length (m)
L_D	dimensionless diagonal position in the right angled bend
L_s	slug length (m)
Q	flow rate (m^3/s)
t	time (s)
U	velocity (m/s)
U_G/U_L	gas/liquid superficial velocity (m/s)
U_{TP}	two-phase superficial velocity (m/s)
U_{abs}	absolute liquid velocity (m/s)
U_b	bubble velocity (m/s)
U_{rel}	relative liquid velocity (m/s) $U_{abs} - U_b$
V	volume (m^3)
w	microchannel width (m)
x^*	relative x -axis position, corresponds to channel height
y^*	relative y -axis position, corresponds to channel width
z^*	relative z -axis position, corresponds to slug length

Greek letters

σ	interfacial tension (N/m)
μ	viscosity (Pa s)
ρ	density (kg/m^3)
β	void fraction

Subscripts

rc	recirculation
TP	two-phase (sum of gas and liquid phase quantity)

Dimensionless numbers

Ca_{TP}	Capillary number $\mu_L U_{TP} / \sigma_L$
Re_{TP}	Reynolds number $\rho_L U_{TP} d_H / \mu_L$

Acknowledgments

This work was supported by the Centre National de la Recherche Scientifique (CNRS) in France and the Academy of Sciences of the Czech Republic (ASCR) in the framework of a bilateral research program (Project no. 22540) and also the Integrated Project IMPULSE (Project no. NMP2-CT-2005-011816), www.impulse-project.net, within the 6th Framework Programme of the European Commission (funding for N. Völkel). The authors also gratefully acknowledge the participation of T. Abadie in some of the experiments.

References

- Abadie, T., Aubin, J., Legendre, D., Xuereb, C., 2011. Hydrodynamics of gas–liquid Taylor flow in rectangular microchannels. *Microfluidics Nanofluidics*. doi:10.1007/s10404-011-0880-8.
- Abdallah, R., Magnico, P., Fumey, B., de Bellefon, C., 2006. CFD and kinetic methods for mass transfer determination in a mesh microreactor. *AIChE J.* 52, 2230–2237.
- Abdallah, R., Meille, V., Shaw, J., Wenn, D., de Bellefon, C., 2004. Gas–liquid and gas–liquid–solid catalysis in a mesh microreactor. *Chem. Commun.*, 372–373.
- Aubin, J., Ferrando, M., Jiricny, V., 2010. Current methods for characterising mixing and flow in microchannels. *Chem. Eng. Sci.* 65, 2065–2093.
- Aubin, J., Völkel, N., Fletcher, D.F., Xuereb, C., 2009. Vortex structure and mixing in meandering microchannels. In: Proceedings of the Second European Process Intensification Conference, GPE-EPIC, Venice, Italy, 17–20, June.
- Chambers, R.D., Holling, D., Spink, R.C.H., Sandford, G., 2001. Elemental fluorine—Part 13. Gas–liquid thin film microreactors for selective direct fluorination. *Lab Chip* 1, 132–137.

- Chung, P.M.Y., Kawaji, M., 2004. The effect of channel diameter on adiabatic two-phase flow characteristics in microchannels. *Int. J. Multiphase Flow* 30, 735–761.
- Cubaud, T., Ho, C.M., 2004. Transport of bubbles in square microchannels. *Phys. Fluids* 16, 4575–4585.
- Dean, W.R., 1927. Note on the motion of fluid in a curved pipe. *Phil. Mag.* 20, 208–223.
- de Mas, N., Gunther, A., Schmidt, M.A., Jensen, K.F., 2003. Microfabricated multiphase reactors for the selective direct fluorination of aromatics. *Ind. Eng. Chem. Res.* 42, 698–710.
- Dogan, H., Nas, S., Muradoglu, M., 2009. Mixing of miscible liquids in gas-segmented serpentine channels. *Int. J. Multiphase Flow* 35, 1149–1158.
- Ehrich, H., Linke, D., Morgenschweis, K., Baerns, M., Jahnisch, K., 2002. Application of microstructured reactor technology for the photochemical chlorination of alkylaromatics. *Chimia* 56, 647–653.
- Fletcher, D.F., Haynes, B., Aubin, J., Xuereb, C., 2009. Chapter 5: modelling of microfluidic devices. In: Hessel, V., Schotene, J.C., Renken, A., Yoshida, J.-I. (Eds.), *Handbook of Micro Reactors*, Vol. A: Fundamentals, Operations & Catalysts, Wiley, Weinheim, pp. 117–144 (Chapter 5).
- Fouilland, T.S., Fletcher, D.F., Haynes, B.S., 2010. Film and slug behaviour in intermittent slug-annular microchannel flows. *Chem. Eng. Sci.* 65, 5344–5355.
- Fries, D.A., Waelchli, S., Von Rohr, P.R., 2008. Gas–liquid two-phase flow in meandering microchannels. *Chem. Eng. J.* 135, S37–S45.
- Fries, D.M., von Rohr, P.R., 2009. Liquid mixing in gas–liquid two-phase flow by meandering microchannels. *Chem. Eng. Sci.* 64, 1326–1335.
- Fujioka, H., Grotberg, J.B., 2004. Steady propagation of a liquid plug in a two-dimensional channel. *J. Biomed. Eng.* 126, 567–577.
- Fukagata, K., Kasagi, N., Ua-arayaporn, P., Himeno, T., 2007. Numerical simulation of gas–liquid two-phase flow and convective heat transfer in a micro tube. *Int. J. Heat Fluid Flow* 28, 72–82.
- Garstecki, P., Fuerstman, M.J., Stone, H.A., Whitesides, G.M., 2006. Formation of droplets and bubble in a microfluidic T-junction—scaling and mechanism of break-up. *Lab Chip* 6, 437–446.
- Günther, A., Khan, S.A., Thalmann, M., Trachsel, F., Jensen, K.F., 2004. Transport and reaction in microscale segmented gas–liquid flow. *Lab Chip* 4, 278–286.
- Gupta, R., Fletcher, D.F., Haynes, B.S., 2010. CFD modelling of flow and heat transfer in the Taylor flow regime. *Chem. Eng. Sci.* 65, 2094–2107.
- Hessel, V., Angelis, P., Gavriilidis, A., Lowe, H., 2005. Gas–liquid and gas–liquid–solid microstructured reactors: contacting principles and applications. *Ind. Eng. Chem. Res.* 44, 9750–9769.
- Inoue, T., Schmidt, M.A., Jensen, K.F., 2007. Microfabricated multiphase reactors for the direct synthesis of hydrogen peroxide from hydrogen and oxygen. *Ind. Eng. Chem. Res.* 46, 1153–1160.
- Jahnisch, K., Baerns, M., Hessel, V., Ehrfeld, W., Haverkamp, V., Lowe, H., Wille, C., Guber, A., 2000. Direct fluorination of toluene using elemental fluorine in gas/liquid microreactors. *J. Fluorine Chem.* 105, 117–128.
- Jaworski, Z., Nienow, A.W., Dyster, K.N., 1996. An LDA study of the turbulent flow field in a baffled vessel agitated by an axial, down-pumping hydrofoil impeller. *Can. J. Chem. Eng.* 74, 3–15.
- Kawahara, A., Chung, P.M.Y., Kawaji, M., 2002. Investigation of two-phase flow pattern, void fraction and pressure drop in a microchannel. *Int. J. Multiphase Flow* 28, 1411–1435.
- Kobayashi, J., Mori, Y., Okamoto, K., Akiyama, R., Ueno, M., Kitamori, T., Kobayashi, S., 2004. A microfluidic device for conducting gas–liquid–solid hydrogenation reactions. *Science* 304, 1305–1308.
- Leclerc, A., Philippe, R., Houzelot, V., Schweich, D., de Bellefon, C., 2010. Gas–liquid Taylor flow in square microchannels: new inlet geometries and interfacial area tuning. *Chem. Eng. J.* 165, 290–300.
- Leung, S.S.Y., Liu, Y., Fletcher, D.F., Haynes, B.S., 2010. Heat transfer in well-characterised Taylor flow. *Chem. Eng. Sci.* 65, 6379–6388.
- Losey, M.W., Schmidt, M.A., Jensen, K.F., 2001. Microfabricated multiphase packed-bed reactors: characterization of mass transfer and reactions. *Ind. Eng. Chem. Res.* 40 (12), 2555–2562.
- Serizawa, A., Feng, Z.P., Kawara, Z., 2002. Two-phase flow in microchannels. *Exp. Therm. Fluid Sci.* 26, 703–714.
- Shah, R.K., London, A.L., 1978. *Laminar Flow Forced Convection in Ducts*. Academic Press Inc., NY.
- Taylor, G.I., 1961. Deposition of a viscous fluid on the wall of a tube. *J. Fluid Mech.* 10, 161–165.
- TeGrotenhuis, W.E., Cameron, R.J., Viswanathan, V.V., Wegeng, R.S., 2000. Solvent extraction and gas absorption using microchannel contactors. *Microreaction Technology: Industrial Prospects*, pp. 541–549.
- Thulasidas, T.C., Abraham, M.A., Cerro, R.L., 1997. Flow patterns in liquid slugs during bubble-train flow inside capillaries. *Chem. Eng. Sci.* 52, 2947–2962.
- Triplett, K.A., Ghiaasiaan, S.M., Abdel-Khalik, S.I., Sadowski, D.L., 1999. Gas–liquid two-phase flow in microchannels—Part I: two-phase flow patterns. *Int. J. Multiphase Flow* 25, 377–394.
- van Steijn, V., Kreutzer, M.T., Kleijn, C.R., 2007. μ -PIV study of the formation of segmented flow in microfluidics T-junction. *Chem. Eng. Sci.* 62, 7505–7514.
- Waelchli, S., von Rohr, P.R., 2006. Two-phase flow characteristics in gas–liquid microreactors. *Int. J. Multiphase Flow* 32, 791–806.
- Yeong, K.K., Gavriilidis, A., Zapf, R., Hessel, V., 2003. Catalyst preparation and deactivation issues for nitrobenzene hydrogenation in a microstructured falling film reactor. *Catal. Today* 81, 641–651.
- Yue, J., Chen, G.W., Yuan, Q., Luo, L.G., Gonthier, Y., 2007. Hydrodynamics and mass transfer characteristics in gas–liquid flow through a rectangular microchannel. *Chem. Eng. Sci.* 62, 2096–2108.
- Yue, J., Luo, L.G., Gonthier, Y., Chen, G.W., Yuan, Q., 2008. An experimental investigation of gas–liquid two-phase flow in single microchannel contactors. *Chem. Eng. Sci.* 63, 4189–4202.
- Yun, J., Lei, Q., Zhang, S., Shen, S., Yao, K., 2010. Slug flow characteristics of gas-miscible liquids in a rectangular microchannel with cross and T-shaped junctions. *Chem. Eng. Sci.* 65, 5256–5263.